

Instrumentation and procedures for validation of synthetic  
infrared image generation (SIG) models

Donna Rankin, C. Salvaggio, T. Gallagher, J. R. Schott

Rochester Institute of Technology, Center for Imaging Science  
P.O. Box 9887, Rochester, New York 14623-0887

ABSTRACT

Synthetic infrared image generation models are becoming more complex with the incorporation of radiation propagation, thermodynamic, environmental, energy matter interaction, and sensor models linked through ray tracers into CAD models of scenes. As these models evolve, it is becoming increasingly necessary and difficult to design validation experiments to determine how well the models work and where the limitations are. This paper describes an experimental approach to validation of the radiometric integrity of an end-to-end thermal infrared SIG model. The approach attempts to break down the overall SIG model into a set of submodels with measurable input and output parameters. A scene is then instrumented and imaged in a time lapse fashion over an extended period (*e.g.*, 48 hours). This scene is also synthetically produced so that the actual and synthetic scenes can be compared. The experimental approach includes acquisition of meteorological data (air temperature, relative humidity, wind speed, cloud cover, precipitation type and rate, total insolation, diffuse insolation), object data (emissivity, absorptivity, thermal conductivity, specific heat, temperature), atmospheric data (transmission, path radiance) and image data (calibrated longwave infrared and midwave infrared images, as well as visible images). Error propagation models are used in conjunction with the experimental data to determine the source and relative importance of errors in the modeling process.

1. INTRODUCTION AND SUMMARY

Infrared scene simulation or synthetic image generation is seeing increasing use in applications, including flight simulation, interpreter aids, analyst training, mission planning, and algorithm development for automatic target recognizers, ATR's. In many of these applications (*e.g.*, flight simulation) it is often sufficient for the images to be reasonably correct radiometrically, as long as general appearance of the image approximates an IR scene. On the other hand, if an analyst is attempting to use SIG to answer "what if" questions, more rigorous thermodynamic and radiometric fidelity is often required. For example, an IRSIG model might be produced to compare with an actual image to determine if the analyst's estimate of what's in the scene would appear the same as what was imaged. For this type of analysis, as well as many of those described above, increasing fidelity is required of the radiometric performance of IRSIG models. The DIRSIG model described by Schott *et al.* 1992<sup>1</sup> is one such model. It accounts for many of the thermodynamic and radiometric phenomena that affect final scene radiance. As a result, the images produced by the model mimic many effects seen in actual imagery.

The focus of this paper is the definition of an approach addressing how well a model such as DIRSIG represents real phenomena in a quantitative sense. In addition, we want to address the obvious follow-up question of what parameters or phenomena are not being adequately modeled so that improvements can be focused where they will have the most impact. An experiment was designed and implemented to acquire the necessary data to test the thermodynamic and radiometric performance of the DIRSIG model, as well as identify what caused any limitations. The experiment consisted of acquiring calibrated time lapse image data of a heavily instrumented scene. The instrumentation included monitoring of meteorological conditions, the temperature of the objects, the atmospheric radiation and transmission levels, and measurements of the optical

properties of the objects in the scene. The experimental scene is then simulated so that the synthetic and actual images can be directly compared in terms of their radiometric fidelity. An error propagation analysis was also performed to determine what parameters were contributing the most to the observed error.

The initial validation results presented here emphasized testing the environmental and thermal model in terms of their ability to predict temperature.

## 2. THE DIRSIG MODEL

There are a variety of thermal infrared synthetic image generation (IRSIG) models described in the literature (*cf.* Cathcart and Sheffer 1991<sup>2</sup>, Biesel and Rohlfing 1987<sup>3</sup>, Kornfeld 1987<sup>4</sup>, Gardner *et al.* 1987<sup>5</sup>). The emphasis here is on IRSIG models attempting to achieve high radiometric fidelity in temperature and radiance predictions (*e.g.*  $\approx 1\text{K}$ ) at high resolutions (*e.g.*  $\approx 1\text{m}$ ). At present there is very little data available for evaluating this type of model. The next section describes procedures for characterizing the radiometric performance of these high resolution models. It is important to recognize that the criteria chosen here is the mean brightness or temperature of objects at the scale of approximately 0.5 to 1 meter. As a result, detailed textural effects within objects are generally not treated. In addition, many investigators (*cf.* Duncan 1990<sup>6</sup> and Lindahl *et al.* 1990<sup>7</sup>) have suggested using a comparison of image derived features measured in an actual image and a synthetic image as a figure of merit. While we believe this approach has merit for evaluating specific feature-based ATR algorithms, it cannot help in addressing thermodynamically-based algorithms or analysis. For example, SIG models aimed at assisting in assessment of signatures, where absolute or even relative temperatures or temperature ranges are important, must be assessed on the basis of radiometric fidelity. Radiometric fidelity is also increasingly important in certain ATR algorithms that include thermodynamic models. And finally, most image derived features will be predicted more faithfully if the image radiometry is correctly simulated. Thus, procedures for evaluating the radiometric fidelity of IRSIG models seems warranted. While each IRSIG model will need to be treated somewhat differently based on its fundamental approach to the problem, we believe a generic model can be adapted which would permit intercomparison of radiometric results. An initial description of this approach is contained in Section 3. However, before proceeding with that discussion we will briefly describe the IRSIG model which will be validated.

The Digital Imaging and Remote Sensing (DIRS) laboratory's image generation model (DIRSIG) is described in greater detail by Schott *et al.* 1992<sup>1</sup>. Figure 2-1 shows an overview of the submodels and input data files that make up the DIRSIG model. The input files consist of a meteorological data file containing data on air temperature, direct insolation, diffuse insolation, wind speed, cloud type, sky exposure, and relative humidity as a function of time for the 24 hours preceding the time of the image to be synthesized. A radiometry data file is produced by a modified version of LOWTRAN to generate transmission, upwelled and downwelled radiance values as a function of view angle and wavelength for each time simulated. The materials file contains optical and thermodynamic data such as angular emissivity, solar absorptivity, specific heat, conductivity *etc.* for each material that exists in the scene. Finally, the scene data file contains a facetized representation of the scene with attributes such as material type and thickness associated with each facet. The scene geometry data file also contains the latitude and longitude of the scene, time of acquisition, and bandpass information. The geometry data file is produced by the image generation submodel which uses the AutoCAD computer aided design (CAD) software to create wire frame representations of objects AutoCAD 1989<sup>8</sup>. The scene generation submodel includes enhancements to AutoCAD to allow the user to assign attributes to facets and to identify the slope, azimuth and normal vector associated with each facet to produce the scene geometry data file. The ray tracer submodel takes the X, Y sensor field of view data, the angular resolution information, and 3-dimensional sensor location and orientation data to

generate a simple camera model. A ray is then cast through each pixel center into the "scene." The ray tracer submodel locates the facet hit and gathers geometric, radiometric, and thermodynamic data about the pixel, background pixels, and the temporal insolation history of the pixel (*i.e.* has it been sunlit or shadowed for the last 24 hours). These data are forwarded to the thermal submodel. The thermal submodel is a modified version of the Therm model described by Spector *et al.* 1991<sup>9</sup> and combines the data from the ray tracer, the 24 hour meteorological data file and the material data file to solve for the current temperature of the pixel. The temperature data, along with the optical and geometric data, are then passed to the radiometric submodel. This submodel uses the data from the other submodels along with the radiometry data file to solve for the radiance reaching the sensor as a function of wavelength. The sensor submodel computes the effective radiance reaching the sensor and converts that radiance into the digital count that would be recorded for that pixel. This process is then repeated for each pixel in the scene until the entire image is produced.

Because the DIRSIG model incorporates both solar and self-emitted radiation propagation, it can be operated to simulate sensors operating in the range from the visible through the longwave infrared. This paper, however, will only treat the thermal infrared characteristics of the model. Figure 2-2 shows a temporal sequence of images generated by the DIRSIG model simulating an 8 to 14  $\mu\text{m}$  image. These images contain essentially no solar reflected energy effects so that the shadows are thermodynamic shadows caused by the cooler temperatures of the ground under the aircraft. Note that much of the contrast, or signature information, in this scene results from thermal shadowing. In order to generate proper target-to-background contrasts and realistic scenes at these resolutions, it will clearly be necessary to have models with high radiometric and thermal integrity. The rest of this paper will focus on the definition of and initial results from a method for evaluating the radiometric performance of IRSIG models in general and DIRSIG in particular.

### 3. APPROACH TO MODEL VALIDATION

In order to evaluate the performance of a synthetic image generation model it is necessary to break the overall SIG modeling processes down into components or submodels and then to divide the submodels into measurable input and output parameters. If a sufficient number of critical input and output parameters can be measured, it becomes possible to not only assess the overall performance of the SIG model, but to identify sources of errors in the submodels or model inputs that cause the final errors. This section will describe the division of the DIRSIG model into testable submodels and the experimental approach and instrumentation used to test the submodels.

#### 3.1 Model components and parameters measured

The components of the DIRSIG model are illustrated in Figure 2-1. The scene geometry submodel is comprised primarily of a standard CAD package modified to accept the addition of material attributes for each facet and to produce an output data structure easily readable by the DIRSIG ray tracer. Its validation comes primarily through verification that the scene elements are properly scaled and oriented and that the material attribute files are being properly accessed. These functions have been verified and will not be treated here.

The ray tracer submodel integrates all the other submodels by tracing each ray into the scene and gathering data to pass on to the thermal and radiometry submodels. It is tested by verifying that the view geometry supplied by the sensor model matches the final image field of view, that shadows and shadow history flags are properly projected, and that specular rays are properly cast to the background. By visual assessment of the image and through use of software debugging tools, the ray interactions were verified. In the same manner, it was verified that the material

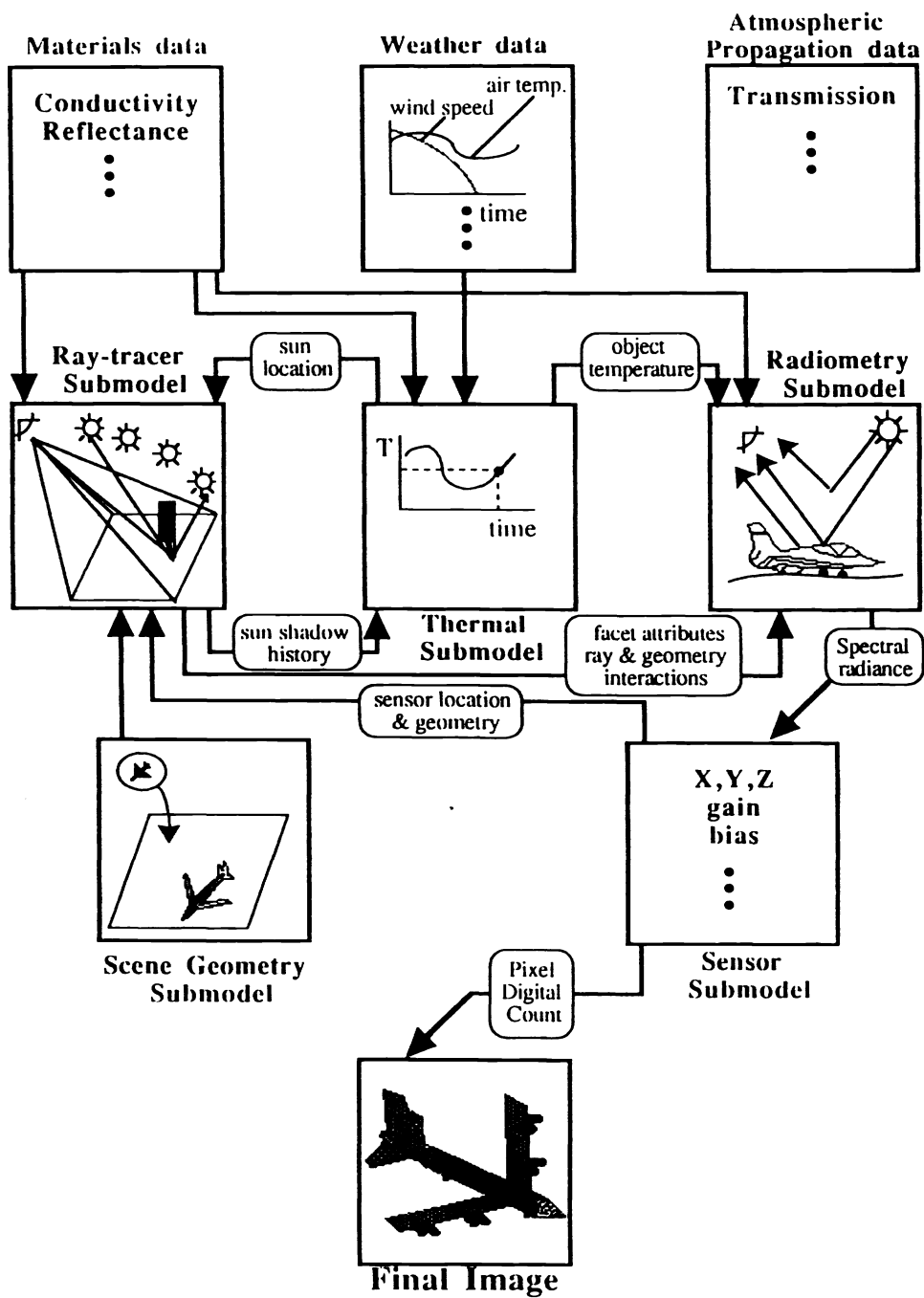


Figure 2-1 Illustration of interactions between submodels in the DIRSIG model



Figure 2-2 8-14  $\mu\text{m}$  synthetic image sequence from 800 to 1500 hours

attributes files were correctly being accessed for the primary and background materials. No further verification of the ray tracer submodel will be considered here.

The primary submodels affecting the radiometric fidelity of the scene are the sensor, thermal, and radiometry submodels. The thermal submodel runs in two modes. In the first mode it takes in 24 hours worth of meteorological data (normally on 15 minutes centers) and the thermodynamic, solar absorption, and orientation properties of the facet. The output of the model is the kinetic temperature of the pixel. This mode is the primary method of operation for research studies where detailed meteorological data are available or where precision results are needed (*e.g.*, for model or algorithm development). The second mode of operation is to use weather forecast data to predict the meteorological inputs. In this mode a limited number of forecast parameters such as estimates of peak air temperature, wind speed, relative humidity, and cloud cover are required along with a longitude, latitude, date, and time. From these inputs 24 hours of meteorological data are generated (normally on 15 minute centers). These data are then used in place of the observed meteorological data to predict the temperature of each facet. In order to validate the thermal submodel, the meteorological data must be measured to determine how well they can be predicted by forecast data. Then the temperature of scene parameters must be measured to determine how well they can be predicted by meteorological data and material parameters. The material parameters are a critical part of this process and can produce considerable error if incorrectly estimated. For this study we will assume that the material parameters are known either from laboratory measurements or field calibration. In the field calibration, unknown material parameters are adjusted to provide a good match to observed temperatures on one day and then those material parameters are used on other days. The input and output parameters for the thermal model are contained in Table 3-1. Also contained in Table 3-1 are the instruments or data sources being used in the validation studies to obtain each parameter. In general the variables in the thermal model which are a function of time (*t*) are sampled at fifteen minute intervals over the course of the validation studies which have typically run 30 to 50 hours. In addition, full meteorological data is normally acquired for an additional 24 hours before a collection because the thermal submodel needs a meteorological history to solve for the current estimate of the temperature of an object. The thermal submodel is validated in both modes. In the first mode the environmental variables are generated as a function of time based on forecast data. In the second mode the meteorological data are measured directly. These data are then combined with materials data, surface orientation, and object background data (*e.g.*, sun shadow history) to predict the surface temperature of objects in the scene. The predictions are normally made as a function of time to monitor how well the model tracks diurnal effects; particularly points of high contrast, contrast reversals, and thermal crossovers. These predictions are validated by comparison with data acquired by thermistor probes attached to scene elements with thermally conductive grease and interfaced to a personal computer for automated data logging. For the studies presented here approximately 12 thermistors recorded data on various objects. Table 3-2 contains a sample listing of the objects monitored on a collection run October 5 and 6, 1990 and June 22 and 23, 1992 along with the material and scene parameters associated with these objects. Figure 3-1 is a diagram of the experimental set up used in the validation. The results of the validation experiment on the thermal model are presented in Section 4.

The radiometric model combines the temperature information from the thermal model with spectral radiometric values for the target, background, sky, and propagation path to solve for the spectral radiance reaching the sensor *cf. Schott et al. 1992*<sup>1</sup>

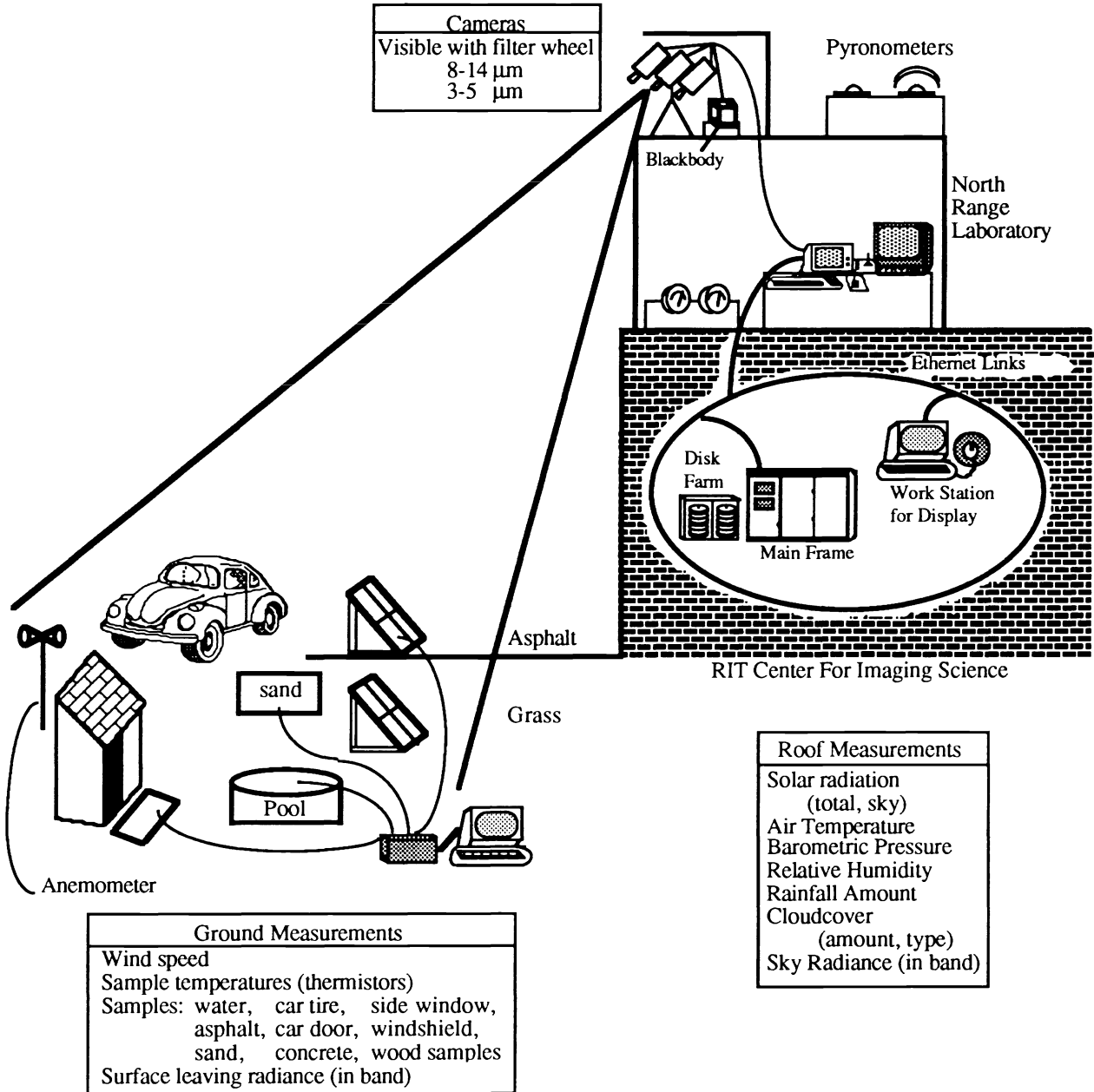


Figure 3-1 Data Collection System

Table 3-1 Thermal Submodel Input/Output Parameters

Inputs to Thermal Model Environmental Prediction		Environmental Model Output Validation		Inputs to Thermal Model Thermodynamic Prediction		Model Output	Validation
Value	Source	Value	Source	Value	Source	Value	Source
Sunrise Time	Longitude, Latitude, Day of Year from Ephemeris	Air Temp(t)	Thermometer (t)	Density	Available Literature	Kinetic Temperature (t)	Thermistor Measurement† (t)
Sunset Time		Air Pressure	Barometer (t)	Specific Heat	Available Literature		
Sunrise Air Temperature	Weather	Relative Humidity	Hygrometer (t)	Thermal Conductivity	Available Literature		
Peak Air Temperature	Service	Dew Point(t)	* (t)	Exposed Area	Experiment Estimate		
Time of Peak Air Temp.	Report	Wind Speed	Anemometer (t)	Visible Emissivity	Available Literature		
Air Pressure		Direct Insolation(t)	Pyranometer* (t)	Thermal Emissivity	Emissometer Measurement		
Humidity		Diffuse Insolation(t)	Pyranometer* (t)	Self-Generated Power	Available Literature		
Dew Point		Sky Exposure	Experimenter Estimate (t)	Thickness	Measurement		
Wind Speed		Cloud Type	Experimenter Estimate (t)	Slope	Measurement		
Sky Exposure		Rain Type	Experimenter (t)	Azimuth	Measurement		
Cloud Type		Rain Rate	Rain Gauge (t)	Sun/Shadow History	Visible Imagery		
Rain Type		Rain Temperature	Experimenter (t)	Plus all of the environmental model outputs and their corresponding experimental values as a function of time			
Rain Rate							
Rain Temperature	Engineering Estimate						

\* Thermal model computes dew point based on air temperature and relative humidity

\*\* Eppley Precision Pyranometers

† YSI Thermistors

The target and background geometric parameters (*e.g.*, material type, pointers to spectral reflectance curves) and the location in the sky from which to draw specularly reflected sky radiance are obtained by the ray tracer. The rest of the radiometric terms are generated by a modified version of LOWTRAN 7 (*cf.* Kneizys *et al.*)<sup>10</sup> which produces spectral values for each term as a function of the relevant parameters (*e.g.*, view angle, time of day). For each scene to be produced, these spectral parameters are entered into a data structure on 100 cm<sup>-1</sup> spectral intervals from which the final values are interpolated (typical values for the interpolation axis are view angle on 0.5 degree centers, sky azimuth on 30 degree centers, and elevation on 15 degree centers). The view angle spacing is a function of the scenario and sensor geometries respectively and can be varied as required. The final effective radiance reaching the scene is computed as

Table 3-2 Object Parameters for Thermistor Samples

Name	Density	Specific Heat	Thermal Conduct.	Thick-ness	Visible Emiss.	Thermal Emiss.	Exposed Area	Self. Power	Slope	Azi-muth
Al.	2.700	.2198	2064	0.0	.15	.10	-1.0	0	45	60
Asphalt	2.114	.2200	5.93	2.4	.93	.93	.40	2.2	0	0
Brick	0.768	.2098	8.17	5.0	.79	.93	-.34	0	45	60
Car Side	7.833	.1111	464.4	.21	.74	.44	1.0	1.45	90	90
Car Roof	7.833	.1111	464.4	.13	.74	.44	.53	0	0	0
Concrete	1.600	.1600	15.48	1.13	.90	.99	-.44	0	42.5	60
Grass	0.160	1.000	0.0	0.0	1.0	.98	.08	1.1	85	180
Gravel	1.000	.3400	17.2	.60	.90	.90	-.375	0	32	60
Sand	1.520	.1911	2.84	1.3	.76	.90	.39	0	0	0
Tire	1.198	.2986	1.3	.15	.93	.90	-.82	0	90	90
Water	1.000	1.000	11.0	14.0	.07	1.0	-.46	0	0	0
Window	1.000	.5200	12.04	.31	.61	.61	.95	.80	67	90
Shield	1.000	.5200	12.04	.11	.61	.61	.52	0	17	180
Wood	0.400	.6689	1.1	2.15	.78	.90	.27	0	32	60

$$L_{\tau_a} = \sum L(\theta, \lambda) \beta(\lambda) \Delta\lambda \tag{1}$$

where  $L(\theta, \lambda)$  is the spectral radiance at view angle  $\theta$ ,  $\beta(\lambda)$  is the normalized spectral response of the sensor,  $\Delta\lambda$  is the wavelength increment, and the sum is over the spectral response range of the sensor.

In summary, the radiometry model takes numerous inputs and predicts the effective radiance reaching the sensor. In order to validate the performance of the model, it is necessary to know the various inputs as well as the final output from the model to determine if errors are in the input parameters or the modeling process. The various inputs to the radiometric model as well as the measurement approach for each one are listed in Table 3-3. In general the major unknowns in the radiometry model are related to atmospheric propagation, target temperature, and the optical properties of the target. The optical properties of the material are assumed known from laboratory measurements based on material type. The atmospheric propagation parameters are obtained by manipulation of LOWTRAN which requires atmospheric profile data to characterize the atmosphere. These data are collected twice a day using radiosondes and then corrected for forecasted or observed surface conditions at the surface during the course of the day. The object and background temperatures are predicted by the thermal model and measured with thermistors for validation. In order to validate the radiometric model, downwelled radiance readings of the sky can be periodically acquired to validate LOWTRAN's estimates of background sky effects. The transmission and path radiance terms can be computed by taking calibrated radiance readings of objects in the scene and in the final image. For these studies this is achieved by periodic radiometer measurements ("ground truth") of several objects. The measurements are made with calibrated field radiometrics spectrally filtered to match the bandpass of the sensor. The sensors are calibrated by having them image a blackbody at various temperatures before and after each frame of imagery (Note: All the sensors used were operated in a fixed gain mode with any automatic gain control circuitry disabled). The digital count can then be related to the radiance sensed by calibration of the sensor gain and bias. This can be expressed as:

$$DC = mL_{T_{bb}} + b \tag{2}$$

Table 3-3 Radiometry Submodel Input/Output Parameters

Inputs to Radiometry Submodel		Validation	Model Output	Validation
Value	Source	Source	Value	Source
ε - Target Emissivity	DIRS Database	Emissometer Measurement	Radiance Reaching the Sensor	Calibrated Radiance Imagery
LT - Target Radiance due to Temp.	Thermal Submodel (Planck)	Thermistor Measurement		
IT & IB Sun/Shadow Histories	Ray_tracer Submodel	Visible Imagery		
Es/p*t1	LOWTRAN	Pyranometer*		
θs - Target Slope	Geometry Submodel	Experimenter Measurement		
F - Shape Factor	Geometry Submodel	Experimenter Estimate		
LD - Downwelled Radiance	LOWTRAN	Spectro-radiometer**		
LTAB - Ave. Background Radiance due to Temp.	Thermal Submodel	Thermistor Measurement		
θB - Background Slope	Geometry Submodel	Experimenter Measurement		
εB - Background Emissivity	DIRS Database	Emissometer Measurement		
τ2 - Target-Sensor Transmission	LOWTRAN	Radiometric Ground Truth		
Lu - Upwelled Radiance	LOWTRAN	Radiometric Ground Truth		
LD^ - Directional LD	LOWTRAN	Spectro-Radiometer**		
Lu^ - Directional Lu	LOWTRAN	Radiometric Ground Truth		
LTB - Background Radiance due to Temp.	Thermal Submodel	Thermistor Measurement		

\* Eppley Precision Pyranometer

\*\* Infrared Systems Spectroradiometer

where DC is the digital count of the image, LTBB is the effective radiance associated with the temperature of the blackbody and, m and b are sensor gain and bias.

From this sensor calibration any digital count in the scene can be converted to effective radiance or apparent temperature. For atmospheric calibration this can be expressed as:

$$L(h, \theta) = \tau(h, \theta)L(0, \theta) + L_u(h, \theta) \tag{3}$$

where  $L(h, \theta)$  is radiance reaching the sensor at elevation  $h$  and view angle  $\theta$  determined from the DC of the image using Equation 2,

$L(0, \theta)$  is the radiance leaving the surface (elevation = 0) into the  $\theta$  direction determined from ground truth radiometers,

$\tau(h, \theta)$  and  $L_u(h, \theta)$  are the slant path transmission and path radiance respectively obtained by

regression of  $L(h,\theta)$  and  $L(0,\theta)$  for comparison with LOWTRAN values.

The optical properties of the materials are generally tested by comparing laboratory measurements of samples from the scene with data base values for parameters such as directional hemispheric emissivity (*cf.* Schott 1986)<sup>11</sup>.

The sensor model used in the current studies only uses fields of view, number of pixels, spectral response, and sensor gain and bias as inputs. The validation is, therefore, focused on verifying that the geometry is correct and that a calibration such as described in Equation 2 is adequate. This is validated by attempting to reproduce blackbody readings for blackbody images other than those used in the calibration process (*cf.*, Table 3-4). In an actual sensor simulation, the optical throughput, sensor noise, radiation by the forward optics *etc.* would also be modeled (*cf.* Schott and Salvaggio 1987).<sup>12</sup>

However, since the emphasis here is on the radiometry reaching the sensor, these effects are not treated.

### 3.2 Error propagation

During the developmental process it is insufficient to know how well a model is performing. It is also necessary to know what the sources of error are so that improvements can be targeted appropriately. In general one would also like to know how much improvement in a particular parameter is necessary in order to achieve a substantial improvement in the overall performance of the model. For example, it would be very useful to know what parameters are the largest sources of error and how much the error will be reduced if the error in that parameter can be reduced a known amount. There are two common ways of conducting such an error analysis. One uses statistical or Monte Carlo methods varying each of the input parameters and recording the variations in output parameters. An alternate method described by Beers 1957<sup>14</sup> uses partial differentials to describe the error in an output term according to

$$s(Y) = \left[ \left( \frac{\partial Y}{\partial X1} s(X1) \right)^2 + \left( \frac{\partial Y}{\partial X2} s(X2) \right)^2 + \dots + \left( \frac{\partial Y}{\partial XN} s(XN) \right)^2 \right]^{1/2} \quad (4)$$

Table 3-4 Sensor Submodel Input/Output Parameters

Inputs to Sensor Submodel		Validation	Model Output	Validation
Value	Source	Source	Value	Source
Sensor Response Function	Manufacturer Specifications	NA	Digital Count	Thermal Imagery
Sensor Gain	BB Calibration Data	BB Imagery		
Sensor Bias	BB Calibration Data	BB Imagery		
Field of View X	User Defined	Visual Inspection of Imagery		
Field of View Y	User Defined			
# of Pixels X	User Defined			
# of Pixels Y	User Defined			

where  $s(Y)$  is the error in the output variable  $Y$  and  $X_1$  through  $X_N$  are the input variable where  $Y$  is a function of  $(X_1, X_2, \dots, X_N)$ . (N.B. If the input variables are dependent on each other, additional cross product terms are required). This approach is very attractive when a governing equation for a model is available because the functional dependencies of the error are explicitly stated. This approach to error analysis is being used for the sensor model and the radiometric model. Because the thermal model uses a sequential equilibrium solution to a time differential heat balance calculation, a closed form solution is impractical. Therefore, a Monte Carlo error propagation approach is used for the thermodynamic model.

This approach to model validation, where nearly every input and output parameter is measured, allows us to not only define how well the models are predicting the final scene, but also through error propagation to determine which submodels or parameters are the source of the error. In this way improvement efforts can be focused on those parameters or submodels which will have the most affect in reducing the final image radiance error.

#### 4. INITIAL RESULTS OF MODEL VALIDATION

Field experiments were conducted on October 5 and 6, 1990 and June 22 and 23, 1992 at RIT's Center for Imaging Science. In addition, field data were available from a U.S.A.F. Wright Labs study described by Spector *et al.* 1991<sup>9</sup>. The early collections emphasized testing field data for the thermal model and often utilized only uncalibrated 8 to 14  $\mu\text{m}$  sensors. The most recent collection employed calibrated visible, near infrared, 3 to 5 and 8 to 14  $\mu\text{m}$  sensors, as well as field and sky radiometers needed for validation of the radiation propagation models. The emphasis thus far has, therefore, concentrated on validation of the thermal model and this paper will reflect that. The validation results presented here for the thermal model are from the RIT collections with analysis and error propagation studies continuing on the entire data set.

The first stage of evaluation of the thermal model was to validate the environmental computations for predicting meteorological values from forecast data. Figures 4-1 and 4-2 show sample results of this study comparing predicted and observed variables. The environmental model works quite well on well-behaved days but has increasing difficulty with overcast days or days with changes in variables such as wind speed with time. These results indicated an expected limitation in the simple forecast approach caused by fixing the value of some of the variables with time (*e.g.*, cloud cover). This limitation is easily corrected by editing the initial estimates of the meteorological variables before object temperature calculations are indicated. For example, if one were attempting to create a scene for 4 p.m. tomorrow based on today's noon forecast of; overcast skies, changing to scattered near midnight, and clearing near dawn with light winds increasing to 10 to 15 mph tomorrow, the meteorological file would be adjusted to account for this additional environmental data. Estimates of how much improvement in target and background temperatures can be obtained using this approach are under way. The results presented here do not include these additional temporal corrections for forecast data. (N.B. The critical parameters; insolation and air temperature vary diurnally based on the environmental models predictions.) For our purposes, the meteorological variables are only important in terms of their influence on final scene temperatures. Therefore, we will not detail the meteorological errors here, only their final impact on temperature.

Typical temperature values as a function of time are plotted in Figure 4-3. These data are indicative of the good performance of the thermal model when actual meteorological data are available and the modest performance when simple forecast data are used (*i.e.*, no correction for temporal changes in forecast). Table 4-1 lists the root mean square (RMS) error between predicted and observed temperature for several samples taken over a range of meteorological conditions over multiple days. These data indicate that temperatures predicted by the model will

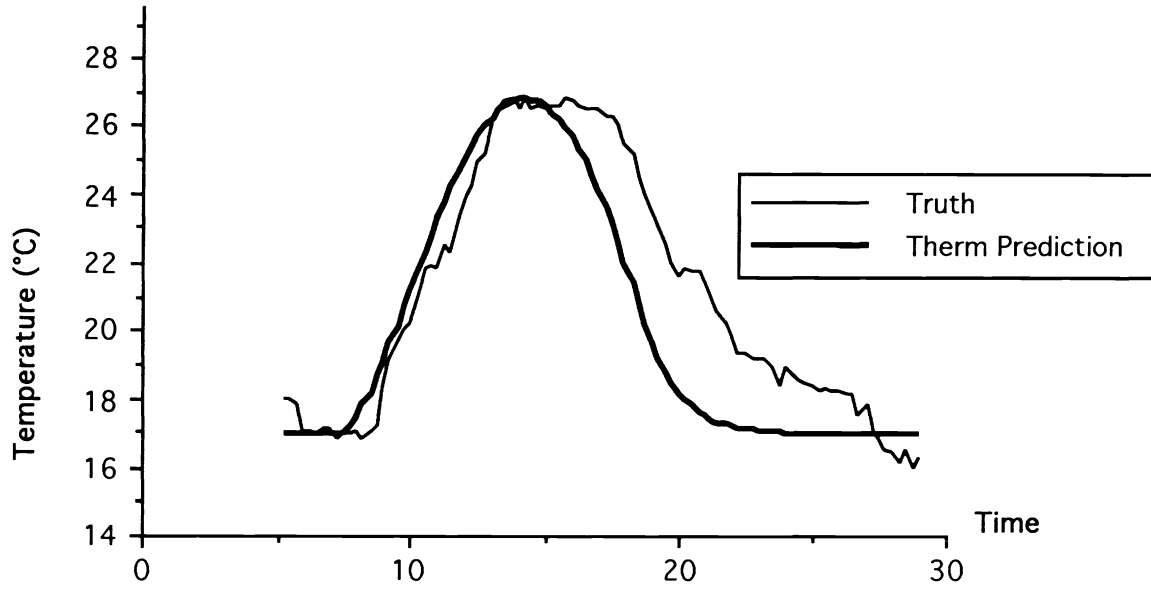


**Figure 4-1 10/6/90 - Air Temperature Truth vs. Therm Prediction**

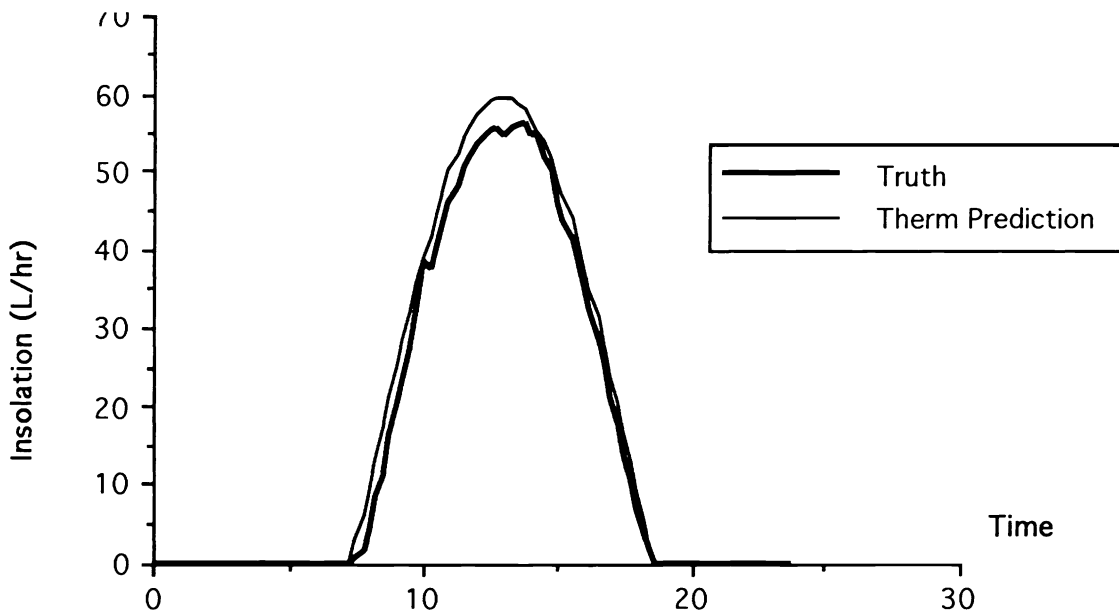


**Figure 4-2 10/6/90 - Direct Insolation Truth vs. Therm Prediction**

**Fig. 4-3a 10/6/90 - Predicted Meteorological Data  
Optimized & Generic vs. Truth**

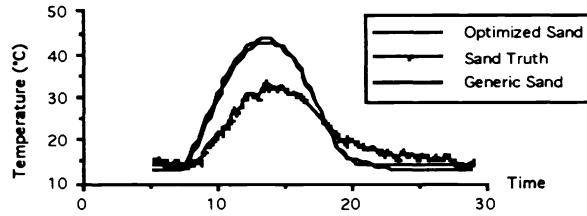


**Fig. 4.3b 10/6/90 - Full Meteorological Data  
Optimized & Generic Parameters vs. Truth**

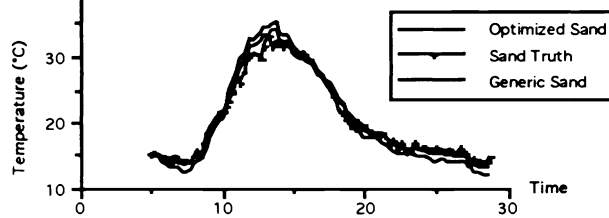


**Fig 4.4a 10/6/90 - Predicted Meteorological Data  
Optimized & Generic Parameters vs. Truth**

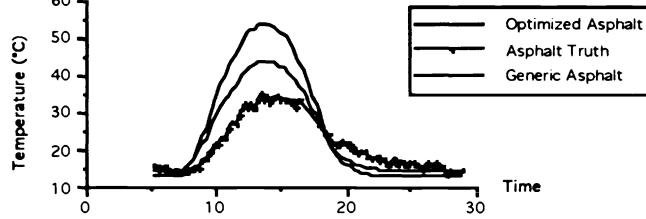


**Fig. 4-4b 10/6/90 - Full Meteorological Data  
Optimized & Generic Parameters vs. Truth**

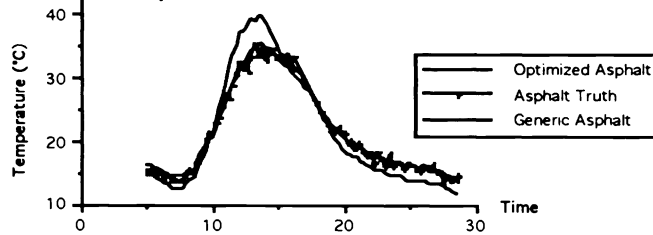


Figure 4-3 Temperature vs. time plots for field optimized and textbook material parameters of sand and asphalt predicted using forecast meteorological data and actual meteorological data.

have an overall RMS error of 1.83K when meteorological data are available and 3.66K when simple forecast data are used with field optimized parameters. In general, better results are obtained under stable clear sky conditions than under variable or overcast conditions. It is important to recognize that for each of the samples in Table 4-1 the material parameters were fixed for all of the days and times included in the study. However, these parameters were adjusted to match the observed thermal conditions when full meteorological data were available.

This indicates that once an object's thermal characteristics are well understood, a data base value should work well in the thermal model. However, for precise estimates "textbook" data base values may be inadequate. For example; if the actual thickness of a sample of concrete is 8 cm, its effective thickness may be better modeled as 6 cm when coupling to lower layers is taken into account. At present only a limited data base of "field calibrated" material parameters exist. "Textbook" values should provide reasonable results, but where precise answers are required, some adjustment based on field simulations is highly desirable. It is also important to note that all the variables tested thus far are passive (*i.e.*, they have no internal heat source). The thermal model used in DIRSIG is designed to emphasize the effects of the environment on passive objects. Since it does not account for lateral conduction, we do not expect its performance on active heat sources to match those reported. Ongoing studies are aimed at quantifying this limitation.

The error analysis conducted to this point indicates that the sources of error when full meteorological data are available are primarily caused by errors due to lack of knowledge of wind speed, solar absorptivity, and exposed area and to a lesser extent air temperature. When the forecast data are used instead of actual weather observations, errors in diffuse insolation, direct insolation, air temperature and absorptivity are the largest contributors to the temperature error.

Ongoing studies are evaluating the radiation propagation aspects of the DIRSIG model and continuing the analysis of the thermal aspects of the model. Future efforts are focusing not only on RMS error, but also on thermal and radiometric contrast error terms. The preliminary evaluation of the radiometric data indicates a good visual correlation between the actual and synthetic data. More quantitative analysis is underway for assessment of the end-to-end performance of the system.

Table 4-1 RMS errors between thermistor truth and prediction values using optimized or generic object parameters for October 6, 1990 and June 23, 1992\*

Object	Observed Meteorological Data		Predicted Meteorological Data	
	Optimized	Generic	Optimized	Generic
Aluminum <sup>1</sup>	1.23	1.52	1.67	5.06
Asphalt <sup>2</sup>	2.31	4.33	5.05	8.14
Brick <sup>1</sup>	1.78	1.90	2.06	5.00
Car Roof (white) <sup>1</sup>	1.63	2.09	2.93	5.94
Car Side (white) <sup>1</sup>	2.91	4.59	2.52	4.15
Car Window <sup>2</sup>	2.49	8.44	7.78	10.58
Concrete Panel <sup>1</sup>	1.04	1.13	1.70	5.25
Roof Gravel <sup>1</sup>	1.36	1.59	1.35	5.30
Sand <sup>2</sup>	1.14	1.45	4.90	5.21
Tire <sup>2</sup>	3.36	6.22	9.49	7.28
Water <sup>1</sup>	1.05	3.45	1.62	7.24
Windshield <sup>2</sup>	2.27	7.24	5.03	9.39
Wood Panel <sup>1</sup>	1.23	1.77	1.54	7.13
Average Error	1.83	3.52	3.66	6.59

\* 24 hours of data included on 15 minute centers

<sup>1</sup> 10/6/90 only (relatively clear, low dynamic range)

<sup>2</sup> Parameters optimized for 6/23/92 (partly cloudy, high dynamic range), results include RMS errors for targets on both days

## 5. REFERENCES

1. J. R. Schott, R. Raqueño, C. Salvaggio, "Incorporation of a time-dependent thermodynamic model and a radiation propagation model into infrared 3-D synthetic image generation," *J. Opt. Eng.*, Vol 31 #7 pp. 1505-1516, July 1992.
2. J. M. Cathcart and A. D. Sheffer, "Generation and application of high-resolution infrared computer imagery," *J. Opt. Eng.*, Vol 30, #11, pp. 1745-1755 (1991).
3. H. Biesel and T. Rohlfig, "Real-time simulated forward looking infrared (FLIR) imagery for training," *Infrared Image Processing and Enhancement*, Marshall R. Weathersby, Editor, *Proc. SPIE* 781, pp. 71-80 (1987).
4. G. H. Kornfeld, "Digital simulation of precise sensor degradations including non-linearities and shift variance," *Infrared Image Processing and Enhancement*, Marshal R. Weathersby, Editor, *Proc. SPIE* 781, pp. 63-70 (1987).
5. G. Y. Gardner, J. Mendelsohn, J. Kim, and W. Reynolds, "A digital scene model for simulation of visual and infrared imagery," *Infrared Image Processing and Enhancement*, Marshal R. Weathersby, Editor, *Proc. SPIE* 781, pp. 81-86 (1987).
6. D. Duncan, "Unified target modeling, validation, and ATR performance evaluation," *Proc. SPIE, Signal and Image Processing Systems Performance Evaluation*, Vol. 1310, 1990.

7. C. Lindahl, T. Cockcroft, T. Derryberry, J. Sigler, M. Yablonski, "Synthetic, multisensor database generation and validation," *Proc. SPIE, Signal and Image Processing Systems Performance Evaluation*, 1990.
8. AutoCAD Release 10 Reference Manual/Autodesk Inc., (1989).
9. D. N. Spector, P. F. Lambeck, S. L. Sheller, S. C. Sawtell, D. K. Rankin, J. R. Schott, "Air Force infrared simulated image models," ERIM Rpt #213400-53-X(II) *Proc. Infrared Information Symposia*, 35, 2, 71-90 (1991).
10. F. X. Kneizys, E. P. Shettle, L. W. Abreu, J. H. Chetwynd, G. P. Anderson, W. O. Gallery, J. E. A. Selby, and S. A. Clough, Users Guide to LOWTRAN 7, *AFGL-TR-88-0177, Environmental Research Papers, No. 1010*, Air Force Geophysics Laboratory, Optical/Infrared Technology Division, Hanscom AFB, Maryland, August 1988.
11. Schott, J. R., "Incorporation of angular emissivity effects in long wave infrared image models," *Proc. SPIE Symposium, Infrared Technology XII*, Vol. 685, San Diego, CA, August 1986.
12. Schott, J. R. and C. Salvaggio, "Inclusion of sensor noise in radiometric models for generation of synthetic long wave infrared images," SPIE's 31st Annual International Technical Symposium on Optical and Optoelectronic Applied Science and Engineering, San Diego, CA, August 1987.
13. Y. Beers, Introduction to the Theory of Error, Addison-Wesley Publishing Company, Inc., Reading MA, 1957.